International Journal of Fatigue 68 (2014) 292–301

Contents lists available at ScienceDirect

International Journal of Fatigue

journal homepage: www.elsevier.com/locate/ijfatigue

Predicting fatigue resistance of nano-twinned materials: Part II – Effective threshold stress intensity factor range

Piyas B. Chowdhury [a], Huseyin Sehitoglu [a,*], Richard G. Rateick [b]

[a] Department of Mechanical Science and Engineering, University of Illinois at Urbana-Champaign, 1206 W. Green St., Urbana, IL 61801, USA
[b] Honeywell Aerospace, 3520 Westmoor St., South Bend, IN 46628, USA

ARTICLE INFO

Article history:
Available online 19 June 2014

Keywords:
Slip irreversibility
Annealing twin
Short crack growth
Microstructure
Fatigue threshold

ABSTRACT

The determination of $\Delta K_{th,eff}$ for fatigue crack growth has been a challenging task. A model is forwarded to assess this parameter in presence of nano-scale twins for Cu, Ni and Al. The model utilizes the concept of irreversibility of crack emitted dislocation glide. Incremental crack extension is formulated on the basis of force balance of continuum dislocations during cyclic flow. Peierls stresses for free and twin boundary restricted glide, computed in Part I, constitute an essential ingredient in devising crack growth threshold founded on relative positions of dislocations. Predicted $\Delta K_{th,eff}$ for relatively short cracks is shown to be substantially enhanced with a refinement in twin lamellar thickness and twin spacing as indicated experimentally in recent literature. The theoretical values of $\Delta K_{th,eff}$ in Ni, Cu and Al are in good agreement with experimental literature for longer cracks as well. Saturation effects are observed in $\Delta K_{th,eff}$ levels with respect to gradual increase in twin nano-dimensions as well as crack length. Mechanistic origin of these observations is discussed.

1. Background

Threshold stress intensity range, ΔK_{th} is the most widely used parameter to assess fatigue crack growth resistance [1]. Nevertheless, experimental determination of this quantity has remained a rather challenging task to-date. Theoretically, there are a significant number of studies in the literature to predict this metric for coarse-grained materials [2–10]. These works have established the importance of different mesoscale factors underlying the physical process of crack growth onset such as lattice frictional stress, slip irreversibility and microstructural obstacles (e.g. grain or twin boundaries). The present study is geared toward developing a model for evaluating effective threshold stress intensity factor range, $\Delta K_{th,eff}$ for nano-materials with annealing twins. Consideration of nano-twinned materials in the current undertaking is of special interest in view of recent literature [11,12] reporting superior damage resistance therein. Existence of enhanced monotonic mechanical properties of twinned nano-materials has been confirmed in previous literature [13,14]. The underlying micromechanics related to the observed macroscopic properties has been addressed in earlier literature [15–17]. In Part I of this work, we have studied the micromechanics of cyclic plasticity associated with a nano-scale twin in a non-continuum framework with a view to isolating its role on an advancing fatigue crack. In particular, we have computed lattice frictional stress influenced by a twin boundary during cyclic flow which serves as one crucial constituent in modeling fatigue crack propagation in the present work. Three fcc materials are considered for study, namely, Ni, Cu and Al. In Part II, we predict nano-scale twin-influenced $\Delta K_{th,eff}$ levels on the basis of cyclic irreversibility of discrete dislocations emanating from a fatigue crack.

It has been proposed that there exist two different ΔK_{th} levels – (a) a microstructural threshold (for short cracks) and (b) a mechanical threshold (for longer cracks) [18]. Fig. 1 illustrates the distinction between the advancement of a short crack at microstructure level (characterized by fluctuating rate) and stable propagation of a microstructure-insensitive longer crack (in Paris regime). The relative size of a microscopic crack and the associated extent of near-tip slip activities are small compared to the host grain dimension (typically several microns) [19]. It progresses by shear mechanism along the critical slip system with maximum resolved shear stress [20] known as the so-called stage I growth mechanism. At this stage, the advancing micro-crack may be completely arrested at a grain level obstacle such as a grain or a twin boundary [7,18,21–26]. Once a small crack is arrested at such an interface, the minimum applied ΔK level required to advance the crack in the adjacent grain is considered the corresponding micro-

* Corresponding author. Tel.: +1 217 333 4112; fax: +1 217 244 6534.
E-mail address: huseyin@illinois.edu (H. Sehitoglu).

http://dx.doi.org/10.1016/j.ijfatigue.2014.06.006
0142-1123/

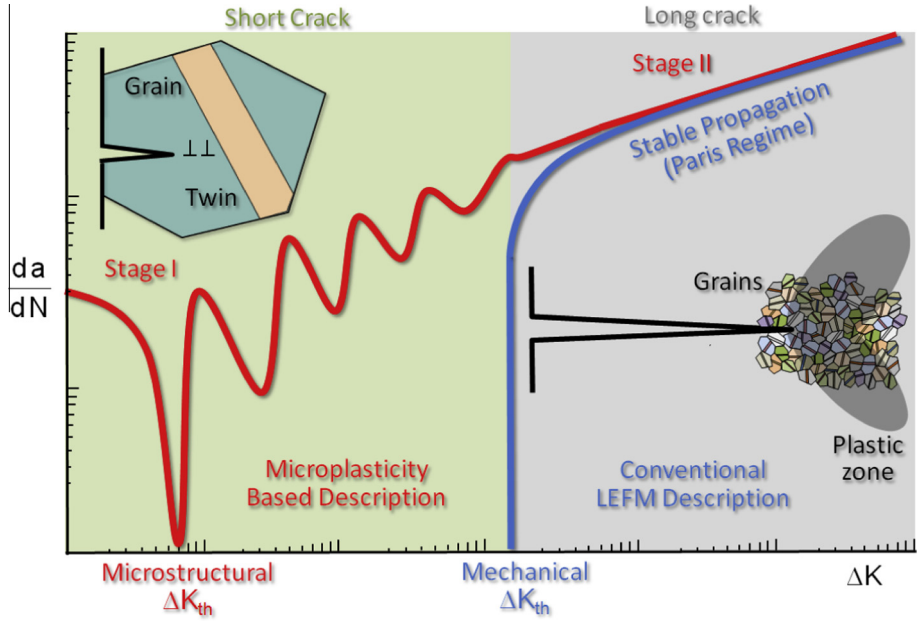

Fig. 1. A schematic demonstrating the crack growth regimes described by conventional linear elastic fracture mechanics (LEFM) and microplasticity. LEFM approach is widely used to characterize the experimentally detectable stable propagation (for long cracks). The mechanical ΔK_{th} is considered as the limiting ΔK level below which no discernible crack growth could be detected by conventional technique. On the other hand, a microscopically advancing crack may be arrested at a grain level obstacle (e.g. a twin boundary) during its early stage of propagation. The microstructural threshold could be deemed as the minimum required ΔK level to advance the crack past such an obstacle. Upon overcoming microstructural ΔK_{th}, the micro-crack progresses with intermittent and subsiding deceleration at various obstacles, eventually to grow long enough to be discerned by LEFM based measurement methods.

structural threshold [18]. Upon overcoming the microstructural threshold, the short crack undergoes periodic retardation at various micro-barriers to a gradually subsiding effect [27]. Therefore, this threshold can be deemed as an important metric representing intrinsic material resistance to cracking as uniquely decided by material microstructure. The behavior of a micro-crack can, therefore, be understood only by considering grain level near-tip microplasticity [28]. Nevertheless, experimental characterization of micro-crack propagation remains a rather challenging task to-date due to limitations of measurement technique at that lengthscale. As a short crack becomes progressively longer, the role of microstructural barriers diminishes until the crack grows sufficiently long to reach a stable propagation stage (the so-called stage II growth or Paris growth regime) [29]. This growth period is characterized by the relative size of crack being significantly larger than individual grains as well as associated plastic zone (accumulated over cycles) which encompasses multitudes of grains. The stage II crack progresses subcritically in a stable manner independent of material microstructure until the catastrophic failure. At this stage, the crack can be physically discerned by conventional detection technique. The microstructure-independent growth of a macroscopically long crack is governed only by applied stress and crack length which can be conveniently described by linear elastic fracture mechanics (LEFM) [30,31]. From a LEFM perspective, the propagation threshold for a macroscopically long crack (i.e. mechanical threshold) is defined as the limiting ΔK level below which no discernible crack advance is detected with the aid of current experimental methods. Therefore, the early stage I growth period for a shorter crack (prior to it becoming noticeably long) is considered as the so-called initiation period for a more detectable longer crack. Evidently, the LEFM-modeled crack growth characterization is dependent on the precision of experimental measurement technique to-date. Nevertheless, these experiments, based on load shedding methods, are subjected to high costs and test matrixes prone to produce data affected by history. In that regard, it is worthwhile to develop a theoretical framework capable of predicting ΔK_{th} at critical microscopic stages which may provide invaluable insight for studying inherent material impedance to cracking. From a theoretical standpoint, a number of works previously undertaken have examined the factors governing the ΔK_{th} discussed as follows.

Upon carefully reviewing earlier threshold models, three distinct categories exist on the basis of slip characteristics as summarized in Table 1 – (i) slip emission, (ii) slip blockage, and (iii) slip irreversibility models. In the slip emission models [3,6,9,10,32], the primary input for threshold prediction consists of the critical shear stress, τ, for dislocation nucleation, crack-tip to dislocation spacing, x, and the relative orientation of the active slip system with respect to the crack path, θ (as shown in the schematic of Table 1). On the other hand, there are a number of experimental observations affirming the role of obstacles such as grain boundaries (GB) on short crack deceleration and/or arrest. GBs provide impedance to the crack-emitted slips, and hence necessitate greater applied shear stress, τ, for further slip emission due to shielding effects. Relative ease of slip transfer across GBs (i.e. complete blockage versus full transmission) strongly depends on the local stress state at the reaction site and the geometry of incident dislocations and GBs [16]. Distinct outcomes of slip-GB reactions would significantly affect the threshold condition. Hence, slip blockage models [4,8,33] considered the difficulties in the forward plastic flow (an enhanced τ), crack length, a_o, and the proximity of the crack-tip to the GB, d, to be the deciding factors for the onset of crack propagation. In these studies, the threshold condition was expressed in terms of the critical ΔK level below which a crack is incapable of transmitting strain to a neighboring grain. Moreover, upon cyclic loading, GBs inflict irreversibility of slip glide which leads to accumulation of permanent strain at crack-tip. Therefore, slip irreversibility models [5,34–38] considered the non-zero differential between the forward and reverse plasticity. The degree of irreversible glide of dislocation dictates the net permanent crack-tip extension i.e. completely reversible cyclic flow would cause no effective crack growth. The interplay with microstructural

Table 1
Summary of notable slip-based ΔK_{th} models in the literature.

Models	Investigators	Threshold	Schematic
Slip emission	[3,6,9,10,32]	$\Delta K_{th} \sim f(\tau, x, \theta)$ τ = critical stress to nucleate slip x = crack-tip to dislocation distance θ = angle between slip and crack path	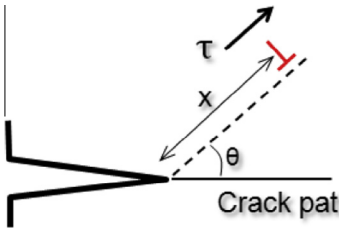
Slip blockage	[4,8,33]	$\Delta K_{th} \sim f(\tau, a_o, d)$ a_o = initial crack length d = crack-tip to GB distance	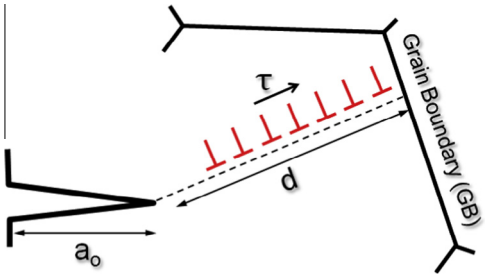
Slip irreversibility	[5,34–38]	$\Delta K_{th} \sim f(\Delta\tau)$ $\Delta\tau$ = forward and reverse flow stress differential	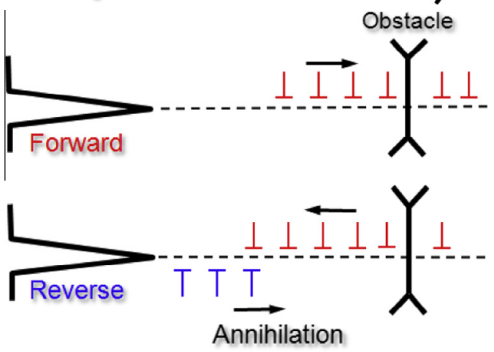

obstacles (e.g. GBs) would modify the extent of slip irreversibilities, thereby affecting the fatigue crack growth onset. Discrete slip model by Pippan et al. [5,35–37], in particular, demonstrated that the dynamic annihilation of dislocations of opposite signs leads to the overall irreversible glide paths. Hence, the interfacial obstacles are found to serve as both slip blockage and slip irreversibility-inducing microstructural elements.

In light of the aforementioned discussion, we note that the physics of microstructure-dependent crack advance involves the combined effects of grain crystallography, lattice resistance to discrete slip glide, and irreversibilities of near-tip and interfacial plasticity. Evidently, the governing metallurgical variables span non-continuum to continuum considerations. Hence, in Part I, we have studied the discrete lattice effects on dislocation glide as influenced by a nano-scale twin. Currently, in Part II of the study, atomistically computed lattice frictional stress from Part I is utilized to predict $\Delta K_{th,eff}$ based on the irreversibility of crack-emitted discrete dislocations as imposed by nano-scale twins.

2. Proposed fatigue crack growth model

In order to estimate twin-induced ΔK_{th} levels, we conduct fracture mechanics based crack growth simulations. Fig. 2 illustrates the configuration used for this purpose. A semi-infinite single crystal with a corner crack is constructed as shown. Twins of finite lamellar thickness, t, and inter-twin spacing, d are placed ahead of the advancing crack. Cyclic farfield loading is applied on the system. A series of elastically interacting dislocations emanate from the crack-tip. The forward and reverse dislocation motions are shown in red[1] and blue.

In this approach, plasticity only ahead of the crack-tip is considered i.e. excluding any wake plasticity. Hence, the ΔK_{th} computed in this manner would essentially be effective threshold stress intensity factor range, $\Delta K_{th,eff}$. Fig. 3 shows the types of the dislocation associated with the respective mode of loading. Mode I and II cracks emit pure edge dislocations while screw dislocations emanate from a mode III crack. These dislocations assume equilibrium positions at the end of forward and reverse loading, balanced by the lattice resistance stress (for free as well as twin-restricted glide). Upon cyclic loading, there is a net irreversibility of dislocation glide trajectories that leads to crack-tip plastic displacement per cycle.

2.1. Cyclic slip irreversibility causing permanent crack extension

Fig. 4 schematically demonstrates the mechanism of the irreversibility of crack-emitted dislocations (for the sake of simplicity, no twin is shown). Upon reversing the load, two scenarios are possible leading to irreversible glide. The crack at the peak of the forward loading (denoted A) has a total of n number of discrete dislocations ahead at their equilibrium positions, denoted by x_i (from the crack-tip) corresponding to the i-th dislocation ($i = 1, 2, 3, \ldots, n$). The crack-tip displacement is a function of net

[1] For interpretation of color in Fig. 2, the reader is referred to the web version of this article.

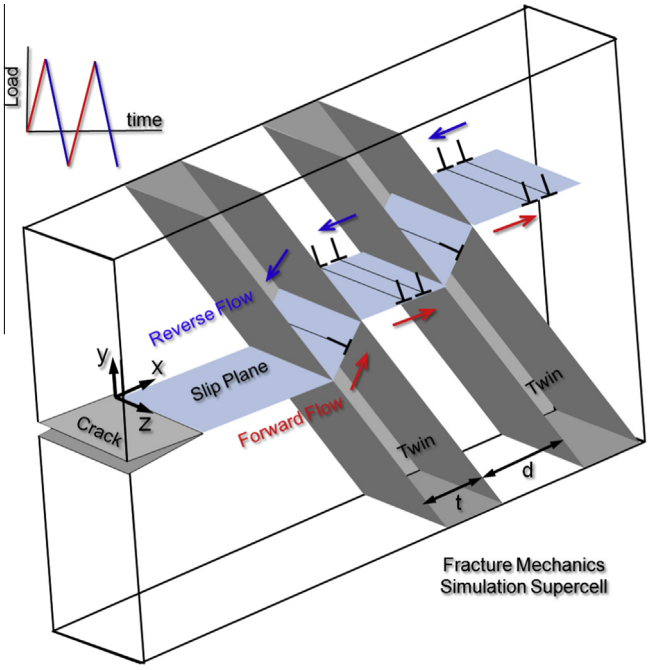

Fig. 2. A semi-infinite body with a corner crack is set up to conduct fracture mechanics simulations. Ahead of the crack, one (or two) twin of finite thickness t is placed. When farfield load (mode I, II or III) is applied on the configuration, the crack emits elastically interacting discrete (mathematical) dislocation. These dislocations assume equilibrium positions, upon overcoming the necessary glide strength (both pristine lattice frictional resistance as well as twin boundary-induced). A formulation for crack growth rate (da/dN) could be derived founded on the differences in forward and reverse dislocation positions (as an outcome of irreversibility due to annihilation).

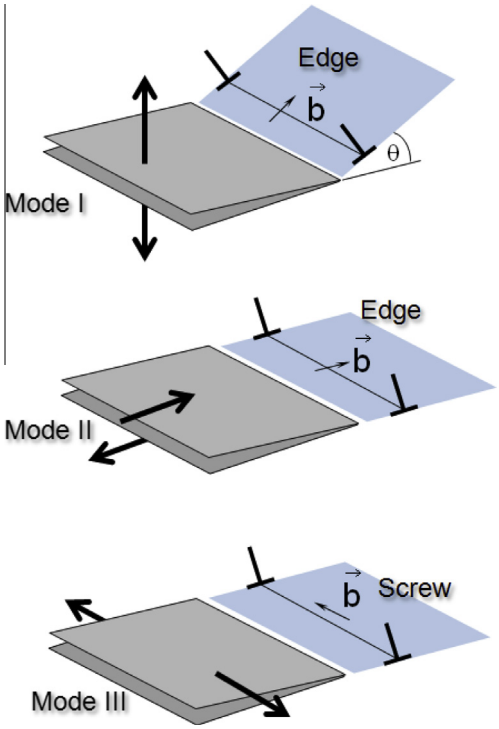

Fig. 3. Different loading modes (I, II and III) and associated dislocation types are illustrated. Mode I and II cracks emit pure edge dislocation while mode III loading generates pure screw dislocation.

irreversible Burgers vectors over a cycle. A permanent displacement corresponding to one Burgers vector (1b), upon complete reversal

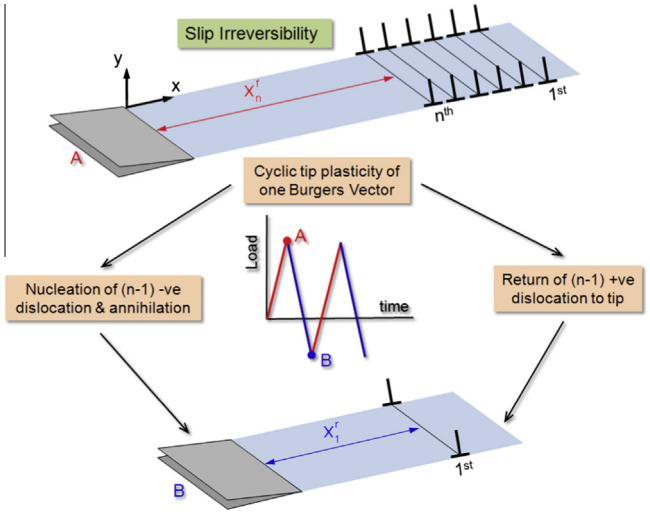

Fig. 4. In order for the crack to commence advancement, a minimum crack growth rate of one Burgers (1b) vector per cycle is required. If n number of dislocations nucleate and assume positions ahead of the crack tip, two distinct possible scenarios may lead to a cyclic tip plasticity equivalent to one Burgers vector. One possibility is the nucleation of $(n-1)$ number of negative dislocations that meet up with the returning dislocations and simultaneously nullifying the positive displacements created at the cracktip, leaving only 1b (corresponding to obstacle placed far away). Another outcome is the return of $(n-1)$ previously nucleated positive dislocations to the crack (no annihilation) with 1b of remaining tip displacement (corresponding obstacle placed close to the crack). In the current model, $\Delta K_{th,eff}$ for the crack advance is defined as the ΔK level corresponding a da/dN of 1b, upon reaching an obstacle.

of load, is necessary to sustain the crack growth at its minimum rate. Below this level, the crack would cease advancing. Such scenario could arise by two possibilities at the end of the reverse loading (designated B). Firstly, $(n-1)$ number of dislocations of opposite sign (labeled 'negative' in the follow-up discussion) can emanate and annihilate the $(n-1)$ crack-bound returning positive slip. It is noted that the nucleation of a negative dislocation along the same slip system from the crack nullifies the step (equal to 1b) created due to the prior positive dislocation emission. Therefore, emission of n number of positive dislocations in forward load and subsequently $(n-1)$ negative slip during reverse load would result in a net cyclic displacement of 1b at the cracktip. Second scenario involves no negative slip nucleation whatsoever and returning of $(n-1)$ positive slip back to the crack-tip. This situation also leaves one dislocation trajectory irreversible (i.e. leading to permanent tip extension corresponding to 1b). The former case is more likely to occur for no obstacle or obstacles placed at a large distance away from the crack-tip, allowing for negative slip nucleation during reverse shear. On the other hand, the latter situation would emerge for the case of an obstacle placed in the close vicinity of the tip, with stronger shielding effects to forward flow (for both positive and negative slip). In the following section, we establish the force balance of dislocations.

2.2. Force equilibrium during dislocation glide

At any stage of loading, the shear stress components acting on the i-th dislocation are: (a) applied shear stress, $\tau_{applied}$ (which drives the dislocation glide from or toward the crack depending on forward or reverse load), (b) image stress, τ_{image} (which always drives the dislocation toward the crack) and (c) pile-up stress, $\tau_{pile\text{-}up}$ (which acts against the glide). Therefore, the net shear stress τ_i acting on the i-th dislocation could be written as follows (where, $i = 1, 2, 3, \ldots, n$; n is the total number of dislocation).

$$\tau_i = \tau_{\text{applied}} - \tau_{\text{image}} - \tau_{\text{pile-up}} \tag{1}$$

The i-th dislocation starts gliding upon overcoming the lattice frictional stress, τ_P which leads to the following equilibrium condition as in Eq. (2).

$$\tau_i \geqslant \tau_P \tag{2}$$

The values of τ_P for free and twin boundary-restricted motion (during forward or reverse glide) have been computed in Table 3 in Part I. The terms, τ_{applied}, τ_{image} and $\tau_{\text{pile-up}}$ can be expressed as a function of dislocation positions, x_i (where, $i = 1, 2, 3, \ldots, n$). Hence, we have Eq. (3) representing the force balance between the net acting shear stress and the lattice resistance for i-th dislocation ($i = 1, 2, 3, \ldots, n$) in a shorthand form.

$$\underbrace{\frac{K}{\sqrt{2\pi x_i}}}_{\text{applied}} - \underbrace{\frac{A}{2x_i}}_{\text{image}} \underbrace{-A\sum_{j\neq i}^{j=n}\sqrt{\left(\frac{x_j}{x_i}\right)}\frac{1}{x_j - x_i}}_{\text{pile-up}} - \tau_P = 0; \quad (i = 1,2,3,\ldots n) \tag{3}$$

where K is stress intensity factor, μ shear modulus, b Burgers vector magnitude, and A is $\frac{\mu b}{2\pi(1-\upsilon)}$ and $\frac{\mu b}{2\pi}$ for edge and screw dislocation respectively (υ is Poisson's ratio). Eq. (3) represents a set of n number of equilibrium expressions for n dislocations. At any instant of loading, all these equilibrium equations are satisfied simultaneously, and solved for x_i for all dislocations. Atomistically computed τ_P levels determine the position of each dislocation under free or twin boundary-restricted glide condition. For instance, when a certain dislocation, upon gliding away from the crack-tip, reaches the twin boundary (located at a particular distance, d), the increased lattice resistance τ_P for forward flow past the boundary (from Table 3 in Part I) is assigned in Eq. (3) for that particular dislocation. Similarly, during reverse flow corresponding Peierls stress at the interface is utilized.

Net irreversible glide path is decided by the final positions at the end of forward and reverse loading (to be defined as x_i^f and x_i^r in the following section). Irreversibility of dislocation glide path eventually causes net plastic displacement at the crack-tip. Hence, in the following section, we derive the cyclic crack growth rate as a function of the final dislocation positions.

2.3. Crack growth rate formulation

Fatigue crack growth rate, da/dN can be computed by the differences in forward and reverse crack-tip displacement (u_f and u_r respectively) along the crack propagation path given by Eq. (4) [34].

$$\frac{da}{dN} = (u_f - u_r)\cos\theta \tag{4}$$

where θ is the angle between the slip plane and crack growth path. In the current model, it has been considered 70° for mode I and zero for mode II and III. The displacements during each half cycle (forward, u_f and reverse, u_r) are given by Eq. (5).

$$du = \frac{1}{2\mu}\int \tau dx \tag{5}$$

In view of the discreteness of dislocations, the integral is replaced by discrete summation, leading to the following expression of u_f and u_r (for $\theta = 0°$) as follows.

$$u_f = \frac{x_1^f}{2\mu}\sum_{i=1}^{i=n}\tau_i^f \tag{6}$$

$$u_r = \frac{x_1^f}{2\mu}\sum_{i=1}^{i=n}\Delta\tau_i^r \tag{7}$$

Delta (Δ) in Eq. (7) indicates that distance parameters during the reverse loading (i.e. crack displacement and dislocations positions, x_i) are computed considering the crack-tip at origin. From Eqs. (4), (6), and (7), we obtain the formulation for da/dN as follows.

$$\frac{da}{dN} = \frac{x_1^f}{2\mu}\sum_{i=1}^{i=n}(\tau_i^f - \Delta\tau_i^r) \tag{8}$$

where x_1^f is the final location of the first emitted dislocation (i.e. $i = 1$) which represents the extent of forward flow activities i.e. plastic zone size. Rewriting Eq. (8) in terms of full expressions of individual shear stress terms (i.e. τ_{applied}, τ_{image} and $\tau_{\text{pile-up}}$), we obtain the final expression for the da/dN as in Eq. (9). (for $\theta = 0°$).

$$\frac{da}{dN} = \frac{x_1^f \Delta K}{2\mu\sqrt{2\pi}}\sum_{i=1}^{i=n}\left(\frac{1}{\sqrt{x_i^f}} - \frac{1}{\sqrt{x_i^f - x_i^r}}\right) - A\frac{x_1^f}{4\mu}\sum_{i=1}^{i=n}\left(\frac{1}{x_i^f} - \frac{1}{x_i^f - x_i^r}\right) - A\frac{x_1^f}{2\mu}\sum_{i=1}^{i=n}\sum_{j\neq i}^{j=n}\left(\sqrt{\left(\frac{x_j^f}{x_i^f}\right)}\frac{1}{x_j^f - x_i^f} - \sqrt{\left(\frac{x_j^f - x_j^r}{x_i^f - x_i^r}\right)}\frac{1}{(x_j^f - x_j^r) - (x_i^f - x_i^r)}\right) \tag{9}$$

Eq. (9) can be used to evaluate da/dN levels as a function of final dislocation positions at the end of forward and reverse loading (x_i^f and x_i^r respectively). It provides a closed form expression for da/dN as a consequence of differences in forward and reverse dislocation positions. The crack advances during the simulations and dislocation evolution occurs ahead of the crack-tip. Upon advancing for substantial number of growth cycles, the remaining dislocation arrays from preceding cycles lead to saturation effects in terms of the crack size (as discussed in the following section).

2.4. Crack growth simulation in presence of nano-twin

As an example, Fig. 5a illustrates the calculation of twin-influenced $\Delta K_{\text{th,eff}}$ levels from da/dN versus ΔK_{II} plots for the case of a mode II crack (edge dislocation) for Ni. In the inset of Fig. 5a, a crack with initial length a_o of 25 μm advances under a constant applied farfield stress range $\Delta\sigma_{xy}$ under a load ratio R equal to −1 i.e. under completely reversed shearing. A twin of preselected lamellar thickness of 35 nm is placed en route to the crack propagation. The left hand side insets depict dislocation arrangements (at $K_{\max}$ and $K_{\min}$) for the advancing crack sufficiently far from the nearest coherent twin boundary (CTB). At $K_{\max}$, a number of dislocations are emitted and piled-up against the CTB. Some dislocations have overcome the CTB resistance for forward flow and positioned themselves inside the twin at an angle to incident slip path. This angle is configured corresponding to the one observed in molecular dynamics simulations during slip transmission past a CTB (for pure edge case) as reported in Part I. As follows from Fig. 5a inset, the farthest transmitted dislocation situated on the other side of the CTB is still far from the right hand side CTB. Upon reversal, the dislocations closest to the crack-tip commence their crack-bound glide. Some of reverse-gliding dislocations return to crack until dislocations of opposite sign emanate and annihilate the rest of the crack-bound slip until reaching $K_{\min}$. The inset configuration at $K_{\min}$ illustrates the dislocation positions at the end of the cycle.

The crack continues to grow until it starts decelerating upon approaching the nearest coherent twin boundary (CTB) on the left. At this interface, the crack growth rate da/dN reaches its minimum value. At the beginning of the simulation, the farfield $\Delta\sigma_{xy}$ level is appropriately adjusted so as to reach a da/dN of one Burgers vector (1b) in the first encounter with the CTB. The dislocation configurations (at $K_{\max}$ and $K_{\min}$) for the crack in very close proximity to the CTB are illustrated in the right hand side inset of Fig. 5a. At $K_{\max}$,

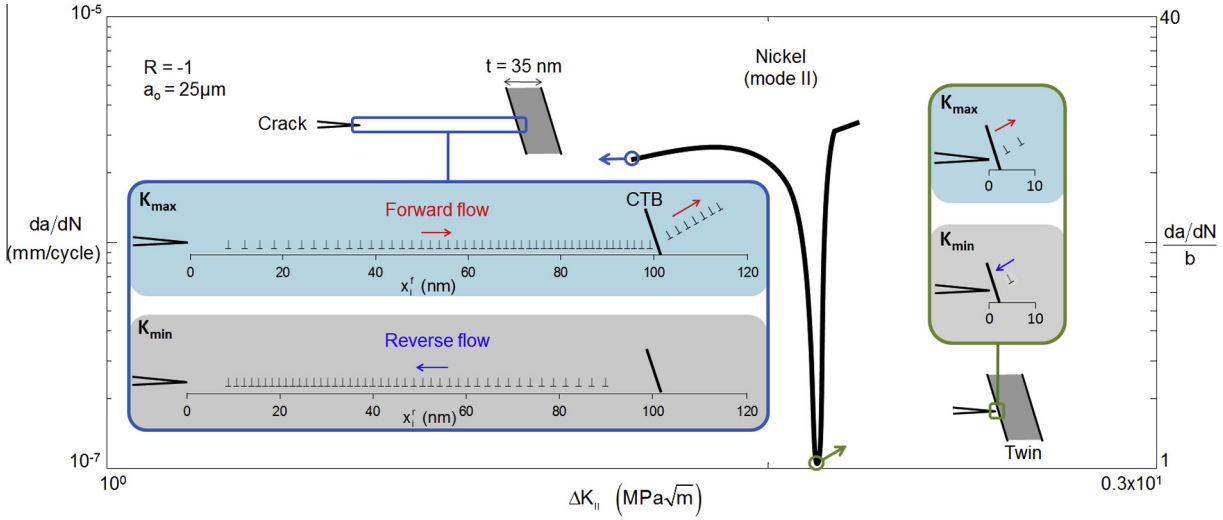

Fig. 5a. *da*/*dN* versus ΔK_{II} plot for a constant twin lamellar thickness (t = 35 nm) simulation for Ni mode II (associated with pure edge dislocation) crack growth. The insets depict dislocation arrangements for the advancing crack sufficiently far from the nearest coherent twin boundary (i.e. left hand side CTB) and when the crack is in very close proximity to the CTB. It follows that *da*/*dN* drops from approximately 23b to 1b as it advances from the former position to the latter. The corresponding dislocation arrangements at K_{max} and K_{min} are illustrated.

two dislocations are emitted and transmitted past the CTB. Upon complete reversal of loading, at K_{min}, one dislocation returns to the crack leaving one transmitted dislocation behind (no dislocation of opposite sign is emitted). During the cycling of σ_{xy}, the crack manages to overcome the CTB resistance and commences its faster propagation through the twin at a rate as high as that prior to encountering the CTB. The ΔK level corresponding to the minimum *da*/*dN* (upon interruption at the first interface) is taken as the $\Delta K_{th,eff}$ for the case of the twin with a particular width t.

Fig. 5b provides a comparison of twin lamellar thickness dependence of thus-computed threshold levels. It follows that a decrease in t shifts thus-computed $\Delta K_{th,eff}$ level to larger magnitudes and results in lowered *da*/*dN* values. This is an outcome of whether the dislocations can reach the second CTB on the right i.e. the relative plastic zone size compared to the twin thickness t. In Fig. 5b insets, the relative extents of plastic zone for small and large magnitudes of t (e.g. 5 and 35 nm) are demonstrated schematically when the crack-tip is resting at the left-hand side CTB. For the case of larger t values (e.g. 5 or 15 nm), the plastic zone size is smaller than the twin thickness. Therefore, the dislocation movement is restricted within a limited volume inside the twin and cannot approach the second (farthest) CTB. On the other hand, for lower t (e.g. 5 or 15 nm), the right-hand side CTB would provide resistance to dislocation glide as the plastic zone extends beyond the twin thickness t.

2.5. Prediction of $\Delta K_{th,eff}$ in nano-twinned Ni, Cu and Al

Fig. 6a provides the $\Delta K_{th,eff}$ levels at different initial crack length a_o values for Ni edge case (mode II). It can be seen that the $\Delta K_{th,eff}$, for a range of twin lamellar thicknesses t (5, 15, 35 and 50 nm), reaches the same saturated level corresponding to a magnitude of about 3.9 MPa$\sqrt{m}$. The effects of different t values are found to be more pronounced at lower magnitudes of a_o (starting from about 130 μm downwards). The differences in $\Delta K_{th,eff}$ at a constant a_o (for example, at 20 μm) become diminishing at gradually larger t (for example, from 5 to 50 nm). The insets show the confinement of dislocation activities within the plastic zone size (cracktip temporarily obstructed at one of the CTBs) and the relative twin lamellar thicknesses. The combined effects of plastic zone extent and the

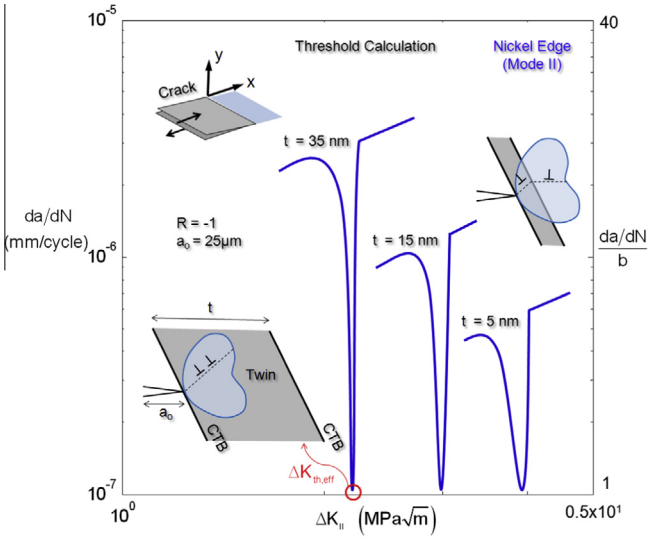

Fig. 5b. Demonstration of currently-employed method of computing $\Delta K_{th,eff}$ from *da*/*dN* versus ΔK curves as influenced by a nano-twin. A crack (of initial length, a_o) located in close proximity to the coherent twin boundary (CTB) is allowed to advance under a constant load ratio ($R = -1$). The farfield applied stress range has been appropriately adjusted to obtain a *da*/*dN* of one Burgers vector at the first encounter with the CTB less than which results in a complete halt of the propagating crack. The crack resumes faster growth once advanced past the CTB. The corresponding ΔK value is considered the $\Delta K_{th,eff}$ for the case of the twin of a particular thickness. The apparent shifts of thus-calculated $\Delta K_{th,eff}$ to larger magnitudes with decreasing t (35 nm 15 nm 5 nm) is associated with a relatively larger plastic zone compared to the twin thickness. As observed, for thinner twins (e.g. 5 nm as shown above), both CTBs obstruct crack-emitted oncoming slip, whereas dislocations cannot reach the far-right CTB in a thicker twin (35 nm) during cyclic flow. It follows from such observation that the $\Delta K_{th,eff}$ level is proportional to the glide impedance provided by a slip-obstacle.

twin thickness determine the observed t-dependence of $\Delta K_{th,eff}$ at lower a_o.

Fig. 6b shows the correlation of $\Delta K_{th,eff}$ on the inter-twin spacing, d. Similar trends (as t-dependence in Fig. 6a) are observed. With refinement in d, the threshold level improves at lower a_o values. Increasing a_o results in a saturated level (of approximately 3.9 MPa$\sqrt{m}$) in $\Delta K_{th,eff}$ for any d values. In the inset schematic,

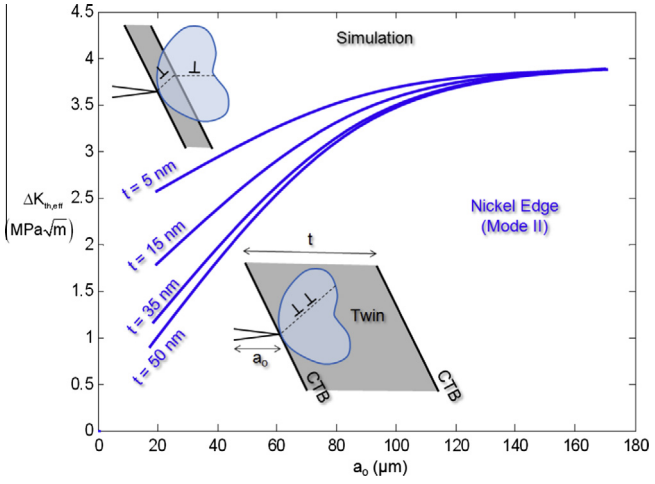

Fig. 6a. $\Delta K_{th,eff}$ as a function of initial crack length (a_o). For cracks shorter than 130 μm, the role of twin thickness t is gradually more prominent. In the short crack regime, with a decrease in t, the threshold levels are improved due to an enhanced resistance to forward flow (when the entire twin is encompassed within the associated plastic zone). Increasing t results in lowered $\Delta K_{th,eff}$ levels with diminishing effects (due to the farthest CTB playing no role in obstructing forward slip). On the other hand, longer cracks thresholds reach a state of obstacle-insensitive advance (corresponding to LEFM-governed stable crack growth regime).

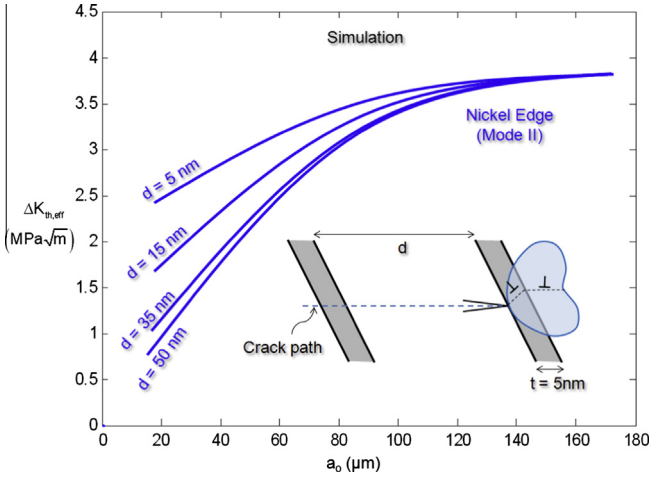

Fig. 6b. Similar to t-dependence of $\Delta K_{th,eff}$, inter-twin spacing d affects the threshold levels for shorter cracks with a diminishing influence for increasing d. The extent of plasticity compared to the relative twin spacing dictates the apparent variation in $\Delta K_{th,eff}$ levels for shorter cracks (<130 μm). Longer crack thresholds saturates toward LEFM-governed magnitudes.

the crack grows through the first twin and approaches the second twin placed at a distance d as shown. The farfield $\Delta\sigma_{xy}$ is selected such that da/dN falls to as low as 1b per cycle at the left-hand side CTB of the twin on the right. At this point, from the da/dN versus ΔK plots, the $\Delta K_{th,eff}$ is calculated, corresponding to the minimum da/dN. In Fig. 6c, a comparison of threshold metrics for Cu, Ni and Al is plotted at a constant t and d values for edge and screw dislocations. It is noted that Ni and Al have the maximum and minimum $\Delta K_{th,eff}$ level respectively which agree well with the experimental findings as depicted. The trend in $\Delta K_{th,eff}$ values for these materials are also found to be consistent with trends observed in terms of the slip irreversibilities and the variations in γ_{us} as reported earlier in Part 1. The minimum slip irreversibility case (Ni edge) corresponds to the maximum resistance to the fatigue crack advancement, manifested in the form of an improved $\Delta K_{th,eff}$.

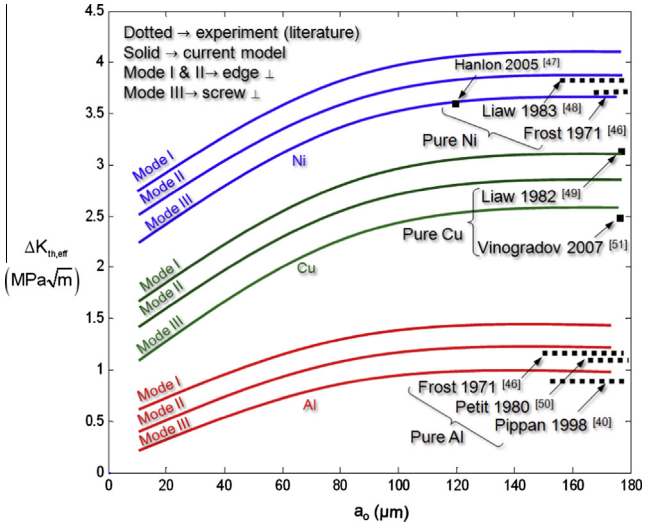

Fig. 6c. A comparison of $\Delta K_{th,eff}$ values for all three materials (Ni, Cu and Al) with experimental data from literature. Model predictions are found to agree well with the available experimental data (mostly for LEFM-governed longer cracks). This indicates the current slip irreversibility based model can successfully reproduce the long crack thresholds, thereby providing validation for shorter crack predictions.

3. Discussion

The concept of cyclic discrete dislocation emission from a fatigue crack has previously been treated in the literature to predict subcritical fatigue crack propagation [2,39]. Pippan et al. [5,35–37,40] proposed a fatigue crack growth model to rationalize the existence of the threshold of crack growth on the basis of a dislocation-mediated crack advance mechanism. They noted that the microstructure-sensitive near-threshold crack growth regime could be accurately modeled only by considering the discreteness of crack-tip plasticity. Early experimental literature have reported observation of near-tip discrete dislocation structures in the metallic single crystals [41,42]. In the present model, we consider the cyclic motions of a series of crack-emitted discrete dislocations gliding on a single slip plane. In the literature, Riemelmoser et al. [37], in particular, have demonstrated that consideration of cyclic flow of crack-emitted discrete slip on several planes culminates in permanent plastic steps along each parallel plane. Therefore, in case of multiple parallel irreversible steps at the crack-tip, the crack blunting process leaves a serrated crack-flank immediately behind the tip. From a physical standpoint, the consequence of these serrations would be manifested as the wake plasticity effect contributing to extrinsic resistance to crack advance (i.e. closure phenomena). Given our objective of capturing the intrinsic crack growth resistance as uniquely posed by material microstructure (i.e. ahead of the crack-tip excluding any wake plasticity), distribution of slip over several parallel glide planes is not considered in the proposed model. The inherent material impedance to fatigue cracking studied in our case (in the form of $\Delta K_{th,eff}$) is a direct consequence of slip activities in front of the crack-tip as influenced by the presence of microstructural obstacles.

The nature of the crack growth process would be significantly altered by the outcomes of slip-obstacle interaction. The effects of micro-barriers would be in particular more dominant for microstructurally short cracks as established in early literature [18]. In that context, the role of nano-scale twins on the fatigue crack growth propagation merits special interest [11,12] due to their apparent contribution to superior damage resistance brought to attention recently. Earlier literature has noted superior ductility as well as strengthening attributes of nano-twinned materials

[14]. It has been reported that there exists a Hall–Petch type effects of twin thickness, t, and spacing, d, on monotonic strength and ductility. Specifically, experimental evidence has indicated superior monotonic mechanical properties with a refinement in t and/or d levels. In the current theory, it has been quantitatively demonstrated that decreasing t and/or d culminates in an improved damage resistance, especially for cracks with shorter initial lengths, a_o. However, the beneficial influences of refined t and d have been found to become saturated at larger magnitudes of these dimensions (as indicated in Figs. 6a–c). This effect could be understood in light of the evolution of twin-induced cyclic slip irreversibilities (detailed investigation of which is documented in the Part I).

If slip-twin boundary reactions promote a reduced degree of irreversibilities, the damage impedance will be enhanced accordingly. As analyzed in Part I, edge and screw type incident dislocations trigger different reaction products at the boundary, and hence different degrees of irreversibilities. The most dominating factor influencing the trends in observed slip irreversibilities have been found to be the relative location of dislocation annihilation with respect to the crack-tip. In particular, the analyses in Part I have unfolded that the residual dislocation plays the role of providing additional resistance to reverse flow, thereby influencing the annihilation location i.e. irreversibility on the whole. However, it is possible to have slip transfer across a twin boundary without any residual dislocation whatsoever, as noted in the literature [16,43]. Direct analysis of such possibility is beyond the scope of this study. Nonetheless, the present analyses (combined Part I and II) provide sufficient mechanistic insight to deduce the expected outcome in such case in terms of crack growth behavior. Intuitively, direct slip transmission case would differ from the present cases (which are transmissions with residual dislocations) in the form of reduced degree of slip irreversibility. Currently computed $\Delta K_{th,eff}$ levels are found to saturate with increasing twin thickness and spacing (for shorter cracks), and eventually with the crack size as in Figs. 6a and b. Therefore, consideration of direct transmission would affect the threshold levels to some extent only for shorter cracks encountering relatively smaller twin thickness and spacing.

From Figs. 6a and b, for a twin thickness or spacing on the order of 35 nm (approximately) or greater, the ΔK_{th} levels converge to a constant magnitude (for a certain a_o) with gradually diminishing t- and/or d-influence. This particular critical value of t and/or d (in the range of 35 nm to 40 nm) can be deemed as an important microstructural length parameter pertinent to twin-induced damage resistance. Moreover, the effects of t and/or d on $K_{th,eff}$ have been found to be predominant only for the cracks with smaller a_o (i.e. $a_o < 130$ μm). With increasing a_o, the effects of twin lamellar thickness or twin spacing on $\Delta K_{th,eff}$ becomes gradually negligible. As such, $\Delta K_{th,eff}$ values are found to have converged to a saturation for larger crack sizes (i.e. $a_o > 130$ μm). The mechanistic origin of such behavior could be rationalized by the physical differences between microstructurally short and long crack advancement processes.

Early literature notes that crack advances of short cracks (i.e. crack size on the order of grain dimension) are more susceptible to retardation and/or arrest by microstructural obstacles [7,18,21–23,25,44]. The growth of such cracks occurs by shear modes along the activated slip direction [20], and is strongly dependent on the extent of near-tip slip activities. In the current model, the extent of short crack plasticity is comparable with the twin lamellar thickness as well as the twin spacing. In the insets of Figs. 6a and b, relative sizes of plastic zones, compared to the twin nano-dimensions, provide a schematic visualization of the range of dislocation activities. The extent of dislocation glide as affected by the presence of the twin boundaries underlies the apparent dependence of $\Delta K_{th,eff}$ on the length parameters t or d. At very large t or d values, the dislocations cannot reach the farthest twin boundary. Therefore, for a twin with a large lamellar thickness, the primary cause of crack growth retardation originates from the first encounter of the crack with the nearest twin boundary. However, smaller t or d allows the farther twin (which is now within the extent of crack-emitted slip glide) to provide additional resistance to the emerging slip, thereby modifying the associated irreversibility upon reversal of loads. This leads to an adjustment to the crack advance resistance manifested in the form of $\Delta K_{th,eff}$ variation with respect to t and/or d.

As the crack length, a_o becomes gradually larger, massive slip accumulation in front of the cracktip is observed to occur which affects the attendant crack advance mechanism. At this stage, the twin boundaries provide almost negligible variation of blockage and/or irreversibility to the multitudes of incident dislocations. Under such circumstances, the plastic zone size is substantially larger compared to twin lamellar width and spacing. Therefore, the extent of crack-originated slip activities encompasses the entire width of a twin of any thickness or twins spaced sufficiently far from each other. Hence, the $\Delta K_{th,eff}$ levels are found to have converged to a saturation independent of crack size, corresponding to microstructure-insensitive stable propagation regime (i.e. for applied stress-driven so-called long crack growth or Paris regime). At saturation, the threshold for longer cracks is no longer dependent on crack length and/or microplasticity (which, on the other hand, is the dominant governing factor for microstructurally short cracks).

The long crack propagation is typically treated in linear elastic fracture mechanics (LEFM) framework with near-tip small scale yielding assumption [4]. It is important to note that the relative size of a long crack plastic zone is significantly larger compared to that of microstructurally small cracks. Nevertheless, in the LEFM consideration, relatively higher dominance of elastic K (stress intensity) fields outside the plastic zone allows for the apparently simplistic conventional treatment of the stable crack growth (i.e. the Paris regime) [45]. In the present analysis, the saturated stage of $\Delta K_{th,eff}$ levels corresponds to this particular stage of massive slip accumulation, thereby rendering the role of microstructural barriers ineffective in influencing the crack advance. Hence, the present microplasticity based considerations can capture the threshold for the microstructure-independent stable crack propagation (i.e. the observed saturated levels), also known as the so-called mechanical threshold (as in Fig. 1). The twin-induced threshold for shorter cracks can, therefore, be deemed as representative of inherent material resistance to damage propagation at micro-level.

Recently, experimental evidence of superior damage properties of nano-twinned Ni–Co alloys has been reported by Sangid et al. [11]. They provided a rationale for the observation in terms of measured cyclic irreversibilities affected by nano-scale coherent annealing twins. Furthermore, Singh et al. [12] have examined pure Cu specially treated to have nano-sized annealing twins in ultrafine-grained specimens (average grain size of approximately 450 nm). Their findings further confirmed the improved fatigue crack growth resistance in nano-twinned ultrafine grained Cu. In particular, they reported a strong dependence of the fatigue crack growth metrics on the twin spacing. A substantial improvement of crack propagation impedance has been observed with the refinement of twin spacings. The conclusions reached through the theoretical framework in the current paper are consistent with the experimental trends observed in recent literature. With a view to validating the current theory, the saturated $\Delta K_{th,eff}$ levels for Cu, Ni and Al (corresponding to the LEFM-governed longer cracks) are matched with earlier experimental findings [40,46–51]. In the literature, a comparison of da/dN versus ΔK of Al, Cu and Ni indicates Ni being most tolerant to damage propagation while Al having least resistance to crack growth [52,53]. The current

microplasticity based theory can capture this trend. The predicted threshold values for longer cracks are in good agreement with the literature data as in Fig. 6c. Direct experimental measurement of the threshold for twin-obstructed short crack propagation has not been conducted as of now to the best of the authors' knowledge. However, materials with increased volume fraction of special grain boundaries (i.e. with high degree of atomic order) are indicated in the literature to have enhanced fatigue resistance, compared to more conventional material microstructure with random grain boundaries [54,55].

Experimentally, grain boundary geometry (i.e. twist and tilt angles) is found to affect the propagation rate by deflecting the crack path [56]. In particular, Lehockey et al. [55] have indicated that the prevalence of low-Σ grain boundaries ($1 < \Sigma \leqslant 29$) in the microstructure lead to a superior fatigue crack propagation impedance (where, Σ is the reciprocal of the fraction of coincident lattice points of two adjoining grain [57]). More recently, Gao et al. [54] have also reported substantial improvement in fatigue crack growth threshold via engineering an increase in the percentage of $\Sigma 3$ grain boundaries (i.e. coherent twin boundaries) in a nickel-base superalloy. The present study provides a physics-based rationale for the experimentally observed damage resistance influenced by $\Sigma 3$ grain boundaries. The present multiscale approach can be viewed as a rapid theoretical assessment of material degradation, especially the role of interfacial slip-barriers therein. In particular, Sangid et al. [58] have studied unstable stacking fault energies for interaction between dislocation and a range of low-Σ grain boundaries on a case by case basis. Part I of the present study has demonstrated the importance of the unstable stacking fault energies in extracting $\Sigma 3$ boundary-induced lattice frictional stresses which are central parameters in predicting the fatigue resistance for the corresponding grain boundary type (as implemented in Part 2). Therefore, as future research, the present methodology (i.e. the proposed combination of atomistic and continuum analyses) could be further extended to incorporate the effects of other grain boundaries, lattice types and materials.

4. Summary and conclusion

In the present work, we have conducted theoretical assessment of fatigue crack growth resistance in presence of nano-scale annealing twins in Ni, Cu and Al. To address the topic, we have devised a fatigue crack growth model based on the irreversibility of elastically interacting discrete dislocation motion from the crack-tip (under mode I, II and II loading conditions). Previously computed (in Part I of this study) twin-restricted lattice frictional stresses govern force balance of these dislocation during cyclic flow. The current analysis (Part II) presents predictions for effective threshold stress intensity factor range, $\Delta K_{th,eff}$ levels for all three materials. The emphasis was given on capturing the transition from the microstructure-sensitive short crack advancement to the so-called longer cracks (typically described by LEFM considerations). The study notes that short crack threshold levels are more pronouncedly affected by nano-scale twins. On the other hand, as the small crack grows progressively longer, the influences of the micro-barriers are markedly diminished. This trend is consistent with the early experimental observations regarding the behavior of microstructurally short cracks and conventional longer cracks. In the current study, such effect is observed to be related to the gradual cyclic accumulation of localized strain at the crack-tip in the form of discrete dislocation arrangement.

Computed $\Delta K_{th,eff}$ levels in Ni, Cu and Al for shorter cracks (approximately less than 130 μm) are found to be strongly correlated with the inter-twin spacing and lamellar thickness. Refinement in twin thickness and/or spacing has been found to favorably affect the crack growth resistance metrics. However, a saturation effect is observed with respect to these twin-related characteristic length parameters, especially for stage I crack growth. With increasing twin width and/or spacing, the beneficial influence on the computed threshold values continues to subside in a saturating manner until reaching a critical value for either of these length parameters (on the order of 50 nm). Beyond this critical value, any additional increase in the twin thickness and/or spacing poses little to no impact on the $\Delta K_{th,eff}$ levels. Such saturation effect is attributed to the gradually increasing relative extent of dislocation activities (i.e. plastic zone size) in comparison with the twin nano-dimensions. Sufficiently thick and/or widely-spaced twins allow limited obstruction to the near-tip flow as the relatively small extent of plasticity precludes the crack-emitted dislocations from reaching the farthest twin boundary. Therefore, the critical twin thickness and/or spacing (i.e. 50 nm), demarcating the onset of saturation, corresponds to a crack advance stage with equal magnitude of plastic zone and either of twin dimensions.

The favorable effects of a nano-scale twin on the threshold measures are dominant until the crack becomes progressively longer to eventually be insusceptible to the presence of slip barriers. The saturation of $\Delta K_{th,eff}$ levels with respect to the crack size is associated with massive near-tip slip arrangements as accumulated over the history of gradual advancement of the crack. Upon reaching a transitional crack size (on the order of 130 μm), $\Delta K_{th,eff}$ levels converge to constant values, irrespective of the twin length parameters as well as the crack size. At this stage, the threshold levels correspond to that of stable long crack growth regime as more traditionally described by the linear elastic fracture mechanics characterization. The long crack $\Delta K_{th,eff}$ magnitudes are observed to be in good agreement with experimental data in the early literature for Ni, Cu and Al.

Acknowledgements

We gratefully acknowledge the support of Honeywell Aerospace Corporation.

References

[1] Suresh S. Fatigue of materials. Cambridge University Press; 1998.
[2] Deshpande VS, Needleman A, Van der Giessen E. Discrete dislocation modeling of fatigue crack propagation. Acta Mater 2002;50:831–46.
[3] Lal DN, Weiss V. A notch analysis of fracture approach to fatigue crack propagation. Metall Trans A 1978;9:413–26.
[4] Navarro A, De Los Rios ER. Short and long fatigue crack growth: a unified model. Philos Mag A 1988;57:15–36.
[5] Pippan R. Dislocation emission and fatigue crack growth threshold. Acta Metall Mater 1991;39:255–62.
[6] Sadananda K, Shahinian P. Prediction of threshold stress intensity for fatigue crack growth using a dislocation model. Int J Fract 1977;13:585–94.
[7] Tanaka K, Hojo M, Nakai Y. Fatigue crack initiation and early propagation in 3% silicon iron. ASTM STP 1983;811:207–32.
[8] Tanaka K, Nakai Y, Yamashita M. Fatigue growth threshold of small cracks. Int J Fract 1981;17:519–33.
[9] Weiss V, Lal DN. A note on the threshold condition for fatigue crack propagation. Metall Mater Trans B 1974;5:1946–9.
[10] Yu W, Gerberich WW. On the controlling parameters for fatigue-crack threshold at low homologous temperatures. Scr Metall 1983;17:105–10.
[11] Sangid MD, Pataky GJ, Sehitoglu H, Rateick RG, Niendorf T, Maier HJ. Superior fatigue crack growth resistance, irreversibility, and fatigue crack growth-microstructure relationship of nanocrystalline alloys. Acta Mater 2011;59:7340–55.
[12] Singh A, Tang L, Dao M, Lu L, Suresh S. Fracture toughness and fatigue crack growth characteristics of nanotwinned copper. Acta Mater 2011;59:2437–46.
[13] Kulkarni Y, Asaro RJ. Are some nanotwinned fcc metals optimal for strength, ductility and grain stability? Acta Mater 2009;57:4835–44.
[14] Lu K, Lu L, Suresh S. Strengthening materials by engineering coherent internal boundaries at the nanoscale. Science 2009;324:349–52.
[15] Christian JW, Mahajan S. Deformation twinning. Prog Mater Sci 1995;39:1–157.

[16] Lee TC, Robertson IM, Birnbaum HK. An In Situ transmission electron microscope deformation study of the slip transfer mechanisms in metals. Metall Trans A 1990;21:2437–47.
[17] Remy L. Twin-slip interaction in fcc crystals. Acta Metall 1977;25:711–4.
[18] Miller KJ. Materials science perspective of metal fatigue resistance. Mater Sci Technol 1993;9:453–62.
[19] Hornbogen E, Gahr K-HZ. Microstructure and fatigue crack growth in a gamma-Fe–Ni–Al alloy. Acta Metall 1976;24:581–92.
[20] Forsyth PJE. Fatigue damage and crack growth in aluminium alloys. Acta Metall 1963;11:703–15.
[21] Lankford J. The growth of small fatigue cracks in 7075-T6 aluminum. Fatigue Fract Eng Mater Struct 1982;5:233–48.
[22] Miller KJ. The behavior of short fatigue cracks and their initiation Part 2 – a general summary. Fatigue Fract Eng Mater Struct 1987;10:93–113.
[23] Pearson S. Initiation of fatigue cracks in commercial aluminium alloys and the subsequent propagation of very short cracks. Eng Fract Mech 1975;7:235–47.
[24] Suresh S, Ritchie RO, Davidson DL, Suresh S. Fatigue crack growth threshold concepts. Warrendale, PA: TMS-AIME; 1984. p. 227.
[25] Taylor D, Knott JF. Fatigue crack propagation behaviour of short cracks; the effect of microstructure. Fatigue Fract Eng Mater Struct 1981;4:147–55.
[26] Brown CW, King JE, Hicks MA. Effects of microstructure on long and short crack growth in nickel base superalloys. Metal Sci 1984;18:374–80.
[27] Morris WL. The noncontinuum crack tip deformation behavior of surface microcracks. Metall Trans A 1980;11:1117–23.
[28] Sheldon GP, Cook TS, Jones JW, Lankford J. Some observations on small fatigue cracks in a superalloy. Fatigue Fract Eng Mater Struct 1980;3:219–28.
[29] James MR, Morris WL, Zurek AK. On the transition from near threshold to intermediate growth rates in fatigue. Fatigue Fract Eng Mater Struct 1983;6:293–305.
[30] Paris PC, Erdogan F. A critical analysis of crack propagation laws. J Basic Eng 1963;85:528–33.
[31] Paris PC, Gomez MP, Anderson WE. A rational analytic theory of fatigue. Trend Eng 1961;13:9–14.
[32] Lanteigne J, Bailon JP. Theoretical model for FCGR near the threshold. Metall Trans A 1981;12:459–66.
[33] Taira S, Tanaka K, Nakai Y. A model of crack-tip slip band blocked by grain boundary. Mech Res Commun 1978;5:375–81.
[34] Wu XJ, Koul AK, Krausz AS. A transgranular fatigue crack growth model based on restricted slip reversibility. Metall Trans A 1993;24:1373–80.
[35] Pippan R. The condition for the cyclic plastic deformation of the crack tip: the influence of dislocation obstacles. Int J Fract 1992;58:305–18.
[36] Riemelmoser FO, Pippan R, Stuwe HP. A comparison of a discrete dislocation model and a continuous description of cyclic crack tip plasticity. Int J Fract 1997;85:157–68.
[37] Riemelmoser FO, Pippan R, Stuwe HP. An argument for a cycle-by-cycle propagation of fatigue cracks at small stress intensity ranges. Acta Mater 1998;46:1793–9.
[38] Wilkinson AJ, Roberts SG. A dislocation model for the two critical stress intensities required for threshold fatigue crack propagation. Scripta Mater 1996;35:1365–71.
[39] Yokobori T, Yoshida M. Kinetic theory approach to fatigue crack propagation in terms of dislocation dynamics. Int J Fract 1974;10:467–70.
[40] Pippan R. The effective threshold of fatigue crack propagation in aluminium alloys. I. The influence of yield stress and chemical composition. Philos Mag A 1998;77:861–73.
[41] Purcell AH, Weertman J. Transmission electron microscopy of the crack tip region of fatigued copper single crystals. Metall Trans 1973;4:349–53.
[42] Mitchell AB, Teer DG. The analysis of dislocation structures in fatigued aluminium single crystals exhibiting striations. Phil Mag 1970;22:399–417.
[43] Couzinie JP, Decamps B, Priester L. Interaction of dissociated lattice dislocations with a sigma 3 grain boundary in copper. Int J Plast 2005;21:759.
[44] Suresh S, Ritchie RO. Propagation of short fatigue cracks. Int Mater Rev 1984;29:445–75.
[45] Smith RA. On the short crack limitations of fracture mechanics. Int J Fract 1977;13:717–20.
[46] Frost NE, Pook LP, Denton K. A fracture mechanics analysis of fatigue crack growth data for various materials. Eng Fract Mech 1971;3:109–26.
[47] Hanlon T, Tabachnikova ED, Suresh S. Fatigue behavior of nanocrystalline metals and alloys. Int J Fatigue 2005;27:1147–58.
[48] Liaw PK, Lea TR, Logsdon WA. Near-threshold fatigue crack growth behavior in metals. Acta Metall 1983;31:1581–7.
[49] Liaw PK, Leax TR, Williams RS, Peck MG. Near-threshold fatigue crack growth behavior in copper. Metall Trans A 1982;13:1607–18.
[50] Petit J, Maillard JL. Environment and load ratio effects on fatigue crack propagation near threshold conditions. Scr Metall 1980;14:163–6.
[51] Vinogradov A. Fatigue limit and crack growth in ultra-fine grain metals produced by severe plastic deformation. J Mater Sci 2007;42:1797–808.
[52] Bansal S, Saxena AM, Hartwig T, Tummala RR. Mechanical properties of ECAE nanocrystalline copper and nickel. J Metastable Nanocrystalline Mater 2005;23:183–6.
[53] Cavaliere P. Fatigue properties and crack behavior of ultra-fine and nanocrystalline pure metals. Int J Fatigue 2009;31:1476–89.
[54] Gao Y, Ritchie RO, Kumar M, Nalla RK. High-cycle fatigue of nickel-based superalloy ME3 at ambient and elevated temperatures: role of grain-boundary engineering. Metall Mate Trans A 2005;36:3325–33.
[55] Lehockey EM, Palumbo G, Lin P. Improving the weldability and service performance of nickel-and iron-based superalloys by grain boundary engineering. Metall Mater Trans A 1998;29:3069–79.
[56] Zhai T, Wilkinson AJ, Martin JW. A crystallographic mechanism for fatigue crack propagation through grain boundaries. Acta Mater 2000;48:4917–27.
[57] Grimmer H, Bollmann W, Warrington DH. Coincidence-site lattices and complete pattern-shift in cubic crystals. Acta Crystallograph Sec A 1974;30:197–207.
[58] Sangid MD, Ezaz T, Sehitoglu H, Robertson IM. Energy of slip transmission and nucleation at grain boundaries. Acta Mater 2011;59:283–96.